Microrheological study of single chain dynamics in semidilute entangled flexible polymer solutions: Crossover from Rouse to Zimm modes

Tsutomu Indei, Tetsuharu Narita

Journal of Rheology 66, 1165 (2022); doi: 10.1122/8.0000402

Microrheological study of single chain dynamics in semi-dilute entangled flexible polymer solutions: Crossover from Rouse to Zimm modes

Tsutomu Indei*

Faculty of Advanced Life Science, Hokkaido University, N21W11, Kita-ku, Sapporo 001-0021, Japan; and Soft Matter GI-CoRE, Hokkaido University, N21W11, Kita-ku, Sapporo 001-0021, Japan

Tetsuharu Narita†

Laboratoire SIMM, UMR7615, ESPCI Paris - CNRS 10 rue Vauquelin, 75005 Paris, France; and Soft Matter GI-CoRE, Hokkaido University, N21W11, Kita-ku, Sapporo 001-0021, Japan

(Dated: January 23, 2023)

Abstract

The dynamics of polymer chains in entangled semi-dilute solution have been of theoretical and experimental interest. Among a number of characteristic lengths and times of the polymer in solution, those of the correlation blob are the key to understand the applicability of the Rouse and Zimm models to rheology of the semi-dilute solution. Direct rheological measurements of Rouse and Zimm modes are limited as the corresponding time scale is out of the range of classical rheological techniques. We investigated the single chain dynamics of entangled poly(ethylene oxide) in semi-dilute aqueous solutions by high-frequency micro-rheology based on diffusing-wave spectroscopy, compared by classical shear macro-rheology. Concentration dependence of the three characteristic times of the entangled polymer chains, reptation time, entanglement time, and correlation time, were studied with the help of the time-concentration superposition (TCS). At the low frequency range, dynamic moduli measured by macro-rheology and micro-rheology showed a good agreement without adjustable parameters. At the higher frequency range, we found the Rouse regime in MSD of the probe particles and in the magnitude of the complex specific viscosity of the solution. We propose a simple method to estimate the boundary of the Rouse regime. Finally, at the high frequency range, we demonstrate that the contribution of the solvent to the solution viscosity needs to be subtracted to observe the power-law behavior of the Zimm mode.

* Correspondence author: indei@sci.hokudai.ac.jp

† Correspondence author: tetsuharu.narita@espci.fr

I. INTRODUCTION

Passive microrheology [1–4] is a relatively new concept and technique in the history of rheology. It can estimate linear viscoelastic properties of soft materials by measuring mean-square displacement (MSD) of thermally fluctuating Brownian particles embedded in the material by using some optical techniques instead of mechanical ones. When the probe particles are larger than the longest characteristic length of the viscoelastic medium, the generalized Stokes-Einstein relation (GSER) can be used to derive the dynamic modulus $G^*(\omega)$ of the medium as a function of the frequency ω from the MSD of the probe particles that is a function of the time t. The GSER is derived by generalizing the conventional Stokes-Einstein relation for Newtonian fluids relating MSD of the probe particles and the solvent viscosity so that it can also treat viscoelastic medium whose rheological property is characterized by the dynamic modulus.

One of the advantages of passive microrheology is its accessibility to high frequency. In conventional oscillatory macro-rheology, upper limit of frequency is about 10^2 rad/s [5]. Though there exists an analytical method to expand the accessible frequency range [6], passive micro-rheology based on dynamic light scattering techniques (single dynamic light scattering, DLS, and mulitple dynamic light scattering, named diffusing-wave spectroscopy, DWS) [1, 3, 7–13] has an advantage at high frequency because it can reach up to almost 10^5 rad/s. Thus high-frequency rheological responses of polymer solutions originating from segmental chain dynamics that reflects its structure can be measured. DWS microrheology has been used to characterize the bending mode of semi-flexible polymers and wormlike micelles, whose high-frequency dynamic modulus exhibits a power-law behavior with an exponent 3/4 [3, 14–17]. The persistence length was calculated from the low-frequency limit of this bending mode. At lower frequency than this bending mode, rheological response of flexible chain was found, which was called the "Rouse-Zimm" mode with an exponent 5/9 [18, 19]. While individual high frequency power-law behaviors having an exponent of 1/2 and/or 2/3 were reported and attributed to the Rouse and/or Zimm mode [11, 13, 20, 21], systematic study on the transition from the Rouse mode to Zimm mode has not been reported to our

best knowledge. The linear viscoelastic behavior of dilute polymer solutions that shows Zimm mode at high frequencies has been measured by macro-rheology [22–24] and evaluated computationally [25] since 1970s. In these experimental studies, zero-concentration limit was taken to study rheological behavior of isolated polymers. Our attempt in this paper is to study rheology of overlapping polymers that is predicted to show crossover from Rouse to Zimm at a certain high frequency due to the correlation length of hydrodynamic interactions that is smaller than polymer size.

In this paper, we report linear rheology of entangled semi-dilute polymer solutions measured by using passive microrheology based on DWS [1, 7]. We use the aqueous solution of high-molecular weight poly(ethylene oxide), PEO, as a model flexible polymer. [26]. While its rheological properties have been extensively studied by both macro-rheology [27–29] and micro-rheology [2, 8, 9, 30], in these microrheological works high frequency properties have not been systematically characterized. We also use conventional macro-rheology in a complemental manner to treat low frequency regime where accuracy of microrheology is reduced. In order to investigate the polymer concentration dependence of the characteristic times and lengths, we use time-concentration superposition (TCS) [27, 31] for both macro- and micro-rheology. By shifting a series of MSD curves plotted against time for some different polymer concentrations vertically and horizontally on log-log scale, a single master curve can be obtained (a part of MSD curves corresponding to concerned dynamic modes can be superposed). Not only the MSD, but also the rheological spectra such as the dynamic modulus and the complex viscosity of the solution plotted against the frequency satisfy the partial TCS.

We focus on the "Rouse-Zimm" mode of flexible polymer and show that the Rouse regime followed by the Zimm regime is distinctly identified in the master curve of the absolute value of the micro-rheological complex specific viscosity $\eta^*_{\rm sp}(\omega)$ at high frequency region where macro-rheology cannot attain. In the Rouse regime, dynamics of the polymer chains is described by the Rouse model [32] for the chain comprised of correlation blobs [33, 34] because some fractions of the chain can move without restrictions within the tube-like domain confining the entire polymer formed by surrounding polymers [35]. On the other hand, in the

Zimm regime, hydrodynamic interactions between polymer segments within the blobs are effective [36]. These regimes are characterized by the exponents derived from the dynamic scaling theory for the Rouse model and Zimm model [34, 35]. In Section II, we briefly review conventional theory for semi-dilute entangled flexible linear polymers [34], which will be used in Section IV to analyze experimental results for PEO aqueous solutions. Experimental details are described and discussed in Section III.

II. THEORETICAL BACKGROUND

In the semi-dilute entangled regime, volume fraction of polymer ϕ satisfies $\phi_{\rm e} < \phi < 1$ where $\phi_{\rm e}$ is the entanglement volume fraction above which polymers feel steric hindrance from the surrounding polymers. Static and dynamic properties of polymer solutions in semi-dilute entangled regime have multiscale hierarchic structure in space and time. Overall features of a wide spectrum of the time/frequency dependence of rheological quantities is ascribed to such multiple scales (see Fig. 1).

A. Characteristic length scales

Spatial (or configurational) hierarchic structure of the solution in semi-dilute entangled regime is characterized by four characteristic length scales; monomer size b, correlation length ξ, tube diameter a, and polymer size $R_{\rm p}$ in increasing order. At the length scale shorter than the monomer size b, solution property is essentially the same as that of solvent. At the length scale larger than b but smaller than the correlation length ξ, solution property is similar to that in the dilute polymer solution where each polymer is separated far apart. At this length scale, hydrodynamic interaction via the solvent and excluded-volume interactions between monomers are effective. In other words, portion of the polymer with size ξ (called correlation blob) is the self-avoiding walk of monomers. If there are g monomers per blob, the blob size is $\xi \approx bg^{\nu}$, where ν is the Flory exponent ($\nu \simeq 0.588$ for good solvent and $\nu = 1/2$ for θ solvent) [34]. Note that the blobs are densely packed and the volume fraction of the polymer within the blob is the same as that of the overall solution, $\phi \approx g(b/\xi)^3$.

Therefore, ξ decreases with increase in ϕ, as

$$\xi \approx b\phi^{-\nu/(3\nu-1)}. \tag{1}$$

In the entangled regime, the tube diameter a, or the distance between the binary interchain contacts, appears as an important length. The tube diameter a is proportional to the correlation length (or size of the correlation blob) ξ, thus scales with the volume fraction as $a \approx a(1)\phi^{-\nu/(3\nu-1)}$ in athermal solvents, where $a(1) \approx bN_{\rm e}(1)^{1/2}$ is the tube diameter in melt ($N_{\rm e}(1)$ is the number of monomers per entanglement strand in melt). Therefore $a \approx \xi N_{\rm e}(1)^{1/2}$ in athermal solvents. On the other hand, $a \approx a(1)\phi^{-2/3} \approx \xi N_{\rm e}(1)^{1/2}\phi^{1/3}$ in θ solvents [34]. At the length scale between ξ and the tube diameter a, both interactions are screened out, and therefore portion of the polymer at this intermediate length scale is formed by the random walk of blobs. Thus polymer size is $R_{\rm p} \approx \xi(N/g)^{1/2}$, where N is the number of monomers per polymer. At the length scale between a and the polymer size $R_{\rm p}$, configuration of the polymer is constrained by the tube-like domain formed by surrounding polymers. Configuration of such entangled polymer is random walk of blobs or random walk of entanglement strands $R_{\rm p} \approx \xi(N/g)^{1/2} \approx a(N/N_{\rm e})^{1/2}$, where $N_{\rm e}$ is the number of monomers per entanglement strand in the solution. At the entanglement volume fraction $\phi_{\rm e}$, tube diameter a ($\approx \xi N_{\rm e}(1)^{1/2}$ in athermal, and $\xi N_{\rm e}(1)^{1/2}\phi^{1/3}$ in θ solvents) is approximately equal to the polymer size $R_{\rm p}$ ($\approx \xi(N/g)^{1/2}$). Therefore, at $\phi \approx \phi_{\rm e}$, $N_{\rm e}(1) \approx N/g$ in athermal, and $\phi_{\rm e}^{-2/3}N/g$ in θ solvents. Considering that $\phi^* \approx N^{-(3\nu-1)}$ and $g \approx \phi^{-1/(3\nu-1)}$, we have

$$N_{\rm e}(1) \approx (\phi_{\rm e}/\phi^*)^{1/(3\nu-1)} \text{ in athermal, and } (\phi_{\rm e}/\phi^*)^{4/3}N^{1/3} \text{ in } \theta \text{ solvents.} \tag{2}$$

B. Characteristic time scales

The dynamic hierarchic structure is characterized by four time scales corresponding to these length scales; relaxation time of monomer τ_0, relaxation time of blob τ_ξ, relaxation time of Rouse subchain $\tau_{\rm e}$ between the consecutive entanglements formed by the blobs, and the reptation time $\tau_{\rm rep}$. In the smallest time scale $t < \tau_0$, rheological property of the solution is essentially the same as that of the solvent. In the second smallest time scale

$\tau_0 < t < \tau_\xi$, rheological property is similar to that in the dilute polymer solution. Therefore hydrodynamic interactions between monomers are effective so that dynamic behavior is represented by the Zimm model [36] that takes account of the hydrodynamic interactions between monomers. In the intermediate time scale $\tau_\xi < t < \tau_\mathrm{e}$, hydrodynamic interactions are screened out and the dynamics is Rouse-like. In the time scale $\tau_\mathrm{e} < t < \tau_\mathrm{rep}$, polymer dynamics is described by one-dimensional diffusion along the tube formed by surrounding polymers (or reptation motion) [35]. Finally, in the longest time scale $t > \tau_\mathrm{rep}$, polymer chains diffuse normally three-dimensionally.

The volume-fraction dependence of these relaxation times has been theoretically studied [33, 34]. The monomer relaxation time is independent of ϕ:

$$\tau_0 \approx \frac{\eta_\mathrm{s} b^3}{k_\mathrm{B} T} \tag{3}$$

where η_s is the solvent viscosity, k_B is the Boltzmann constant and T is the solution temperature. The Zimm relaxation time of blob is governed by the blob size (or correlation length) ξ:

$$\tau_\xi \approx \frac{\eta_\mathrm{s} \xi^3}{k_\mathrm{B} T} \approx \tau_0 \phi^{-3\nu/(3\nu-1)}. \tag{4}$$

The Rouse relaxation time of ideal chain formed by blobs is

$$\tau_\mathrm{e} \approx \tau_\xi \left(\frac{N_\mathrm{e}}{g}\right)^2 \approx \tau_0 N_\mathrm{e}(1)^2 \phi^{-3\nu/(3\nu-1)} \text{ in athermal, and } \tau_0 N_\mathrm{e}(1)^2 \phi^{-5/3} \text{ in } \theta \text{ solvents.} \tag{5}$$

The reptation model predicts that the reptation time τ_rep is proportional to the cube of the molar mass. That is,

$$\tau_\mathrm{rep} \approx \tau_\mathrm{e} \left(\frac{N}{N_\mathrm{e}}\right)^3 \approx \tau_0 \frac{N^3}{N_\mathrm{e}(1)} \phi^{3(1-\nu)/(3\nu-1)} \text{ in athermal, and } \tau_0 \frac{N^3}{N_\mathrm{e}(1)} \phi^{7/3} \text{ in } \theta \text{ solvents.} \tag{6}$$

It is known that experimentally one finds the exponent about 3.4. This difference is explained by the fluctuations of the tube length [35]. The relaxation time deviates from the model prediction especially at low molar mass, leading to stronger molar mass dependence.

C. Relaxation modulus

The conventional theory predicts that the relaxation modulus of entangled semi-dilute solution of linear polymer in athermal solvents (where $\nu = 0.588$) and θ solvents ($\nu = 1/2$)

is approximately

$$G(t) \approx \begin{cases} \frac{k_{\rm B}T}{b^3}\phi(t/\tau_0)^{-1/(3\nu)} & (\text{for } \tau_0 < t < \tau_\xi) \\ \frac{k_{\rm B}T}{\xi^3}(t/\tau_\xi)^{-1/2} & (\text{for } \tau_\xi < t < \tau_{\rm e}) \\ \frac{k_{\rm B}T}{a^2\xi} & (\text{for } \tau_{\rm e} < t < \tau_{\rm rep}) \end{cases} . \tag{7}$$

At specific times $t = \tau_0,\ \tau_\xi,\ \tau_{\rm e}$, it becomes

$$G(t) \approx \begin{cases} \frac{k_{\rm B}T}{b^3}\phi\ (\equiv G_0) & (\text{at } t = \tau_0) \\ \frac{k_{\rm B}T}{\xi^3} \approx \frac{k_{\rm B}T}{b^3}\phi^{3\nu/(3\nu-1)}\ (\equiv G_\xi) & (\text{at } t = \tau_\xi) \\ \frac{k_{\rm B}T}{a^2\xi} \approx \frac{k_{\rm B}T}{b^3}\frac{1}{N_e(1)}\phi^{3\nu/(3\nu-1)} \text{ in athermal, and} & \\ \qquad \frac{k_{\rm B}T}{b^3}\frac{1}{N_e(1)}\phi^{7/3} \text{ in } \theta \text{ solvents } (\equiv G_{\rm e}) & (\text{at } t = \tau_{\rm e}) \end{cases} . \tag{8}$$

These characteristic moduli are given by $k_{\rm B}T$ per corresponding characteristic volume, that is, average volume per monomer b^3/ϕ (at $t = \tau_0$), occupied volume of blob ξ^3 (at $t = \tau_\xi$), and occupied volume of entanglement strand $a^2\xi$ (at $t = \tau_{\rm e}$).

D. Complex specific viscosity

Polymer contribution of the complex viscosity is obtained by subtracting the solvent viscosity $\eta_{\rm s}$ from the complex viscosity of the solution $\eta^*(\omega) = G^*(\omega)/(i\omega)$. The dynamic modulus $G^*(\omega)$ is related to the relaxation modulus $G(t)$ through the one-sided Fourier transformation [22]. We define the complex specific viscosity

$$\eta^*_{\rm sp}(\omega) \equiv \frac{\eta^*(\omega) - \eta_{\rm s}}{\eta_{\rm s}} = \frac{\eta'(\omega) - \eta_{\rm s}}{\eta_{\rm s}} - i\frac{\eta''(\omega)}{\eta_{\rm s}}, \tag{9}$$

and analyze its magnitude $|\eta^*_{\rm sp}(\omega)| = \sqrt{\left[\frac{\eta'(\omega)-\eta_{\rm s}}{\eta_{\rm s}}\right]^2 + \left[\frac{\eta''(\omega)}{\eta_{\rm s}}\right]^2}$ where $\eta'(\omega)$ and $\eta''(\omega)$ are the real and imaginary parts of $\eta^*(\omega)$, respectively.

Corresponding to the relaxation modulus given by Eq. (7), magnitude of the complex specific viscosity in athermal solvents is expected to behave as (see Fig. 1 top)[37]

$$|\eta^*_{\rm sp}(\omega)| \approx \begin{cases} N_{\rm e}(1)(\tau_{\rm e}\omega)^{-1} & (\text{for } 1/\tau_{\rm rep} < \omega < 1/\tau_{\rm e}) \\ (\tau_\xi\omega)^{-1/2} & (\text{for } 1/\tau_{\rm e} < \omega < 1/\tau_\xi) \\ \phi(\tau_0\omega)^{-(1-1/(3\nu))} & (\text{for } 1/\tau_\xi < \omega < 1/\tau_0) \end{cases} . \tag{10}$$

At specific frequencies $\omega = 1/\tau_{\rm rep}, 1/\tau_{\rm e}, 1/\tau_\xi, 1/\tau_0$, it becomes

$$|\eta^*_{\rm sp}(\omega)| \approx \begin{cases} G_{\rm e}\tau_{\rm rep}/\eta_{\rm s} \approx \frac{1}{N_{\rm e}(1)^2}(\phi/\phi^*)^{3/(3\nu-1)} \ (\approx \eta_{\rm sp}) & (\text{at } \omega = 1/\tau_{\rm rep}) \\ G_{\rm e}\tau_{\rm e}/\eta_{\rm s} \approx N_{\rm e}(1) & (\text{at } \omega = 1/\tau_{\rm e}) \\ G_\xi\tau_\xi/\eta_{\rm s} \approx 1 & (\text{at } \omega = 1/\tau_\xi) \\ G_0\tau_0/\eta_{\rm s} \approx \phi & (\text{at } \omega = 1/\tau_0) \end{cases} . \tag{11}$$

On the other hand, magnitude of the complex specific viscosity in θ solvents is (see Fig. 1 bottom)

$$|\eta^*_{\rm sp}(\omega)| \approx \begin{cases} N_{\rm e}(1)\phi^{2/3}(\tau_{\rm e}\omega)^{-1} & (\text{for } 1/\tau_{\rm rep} < \omega < 1/\tau_{\rm e}) \\ (\tau_\xi\omega)^{-1/2} & (\text{for } 1/\tau_{\rm e} < \omega < 1/\tau_\xi) \\ \phi(\tau_0\omega)^{-1/3} & (\text{for } 1/\tau_\xi < \omega < 1/\tau_0) \end{cases} . \tag{12}$$

At $\omega = 1/\tau_{\rm rep}, 1/\tau_{\rm e}, 1/\tau_\xi, 1/\tau_0$, it becomes

$$|\eta^*_{\rm sp}(\omega)| \approx \begin{cases} G_{\rm e}\tau_{\rm rep}/\eta_{\rm s} \approx \frac{N^{2/3}}{N_{\rm e}(1)^2}(\phi/\phi^*)^{14/3} \ (\approx \eta_{\rm sp}) & (\text{at } \omega = 1/\tau_{\rm rep}) \\ G_{\rm e}\tau_{\rm e}/\eta_{\rm s} \approx \frac{N_{\rm e}(1)}{N^{1/3}}(\phi/\phi^*)^{2/3} & (\text{at } \omega = 1/\tau_{\rm e}) \\ G_\xi\tau_\xi/\eta_{\rm s} \approx 1 & (\text{at } \omega = 1/\tau_\xi) \\ G_0\tau_0/\eta_{\rm s} \approx \phi & (\text{at } \omega = 1/\tau_0) \end{cases} . \tag{13}$$

Figure 1 shows schematics of $|\eta^*_{\rm sp}(\omega)|$ as a function of ω on log-log scale for both athermal and θ solutions. Hierarchical structure of polymer solution can be explained in terms of rheology by using Fig. 1 as follows. (Although our main interest is in entangled regime, we begin the explanation with the dilute regime from a pedagogical point of view.) In dilute regime $\phi < \phi^*$ (three blue lines), the Zimm relaxation time of a single polymer chain (denoted by $\tau_{\rm Z}$) is the longest relaxation time. That is, $\omega < 1/\tau_{\rm Z}$ is the terminal flow regime (I) and $\omega > 1/\tau_{\rm Z}$ is the Zimm regime (II) where hydrodynamic interactions are effective. With increasing polymer concentration ϕ, $|\eta^*_{\rm sp}|$ increases but the Zimm relaxation time $\tau_{\rm Z}$ is constant as indicated by upward-pointing arrow from point A because polymers are still isolated. At the overlapping volume fraction $\phi = \phi^*$, blobs start to be generated so that $\tau_{\rm Z}$ is "separated" at point B into the relaxation time of blob τ_ξ and the longest relaxation of the chain formed by blobs $\tau_{\rm chain}$. In unentangled semi-dilute regime $\phi^* < \phi < \phi_{\rm e}$ (three green lines), with increasing ϕ, number

of blobs increases while size of a blob decreases. Consequently, τ_{chain} increases (indicated by the arrow pointing upper-left) whereas τ_ξ decreases (indicated by right-pointing arrow). Such a separation of the relaxation time from τ_{Z} to τ_{chain} and τ_ξ generates a new relaxation mode between them (III) associated with Rouse dynamics of chains formed by blobs. At the entanglement volume fraction $\phi = \phi_{\text{e}}$, entanglements start to be generated so that τ_{chain} is further separated at point C into the relaxation time of the entanglement strands τ_{e} and the longest relaxation of the chain or the reptation time τ_{rep}. Finally, in entangled semi-dilute regime $\phi_{\text{e}} < \phi \ll 1$ (three red lines), number of entanglements strands increase with increasing ϕ while size of tube diameter decreases. As a result, τ_{rep} increases (indicated by the arrow pointing upper-left) while τ_{e} decreases (indicated by right-pointing arrow). Such a separation of the relaxation time from τ_{chain} to τ_{rep} and τ_{e} gives rise to a new relaxation mode between them (IV) related to the reptation dynamics.

Boundaries between two adjoining regimes can be derived by regarding ϕ as the intermediate variable between $|\eta^*_{\text{sp}}|$ and the related relaxation time (for example, for the boundary between I and IV, τ_{rep}). By eliminating ϕ to relate $|\eta^*_{\text{sp}}|$ and the relaxation time, and then by replacing the relaxation time with $1/\omega$, we can obtain the boundary. For athermal solvents, the boundary between I and IV is given by $|\eta^*_{\text{sp}}(\omega)| \approx \frac{N_{\text{e}}(1)^{(2\nu-1)/(1-\nu)}}{N^{3\nu/(1-\nu)}}(\tau_0\omega)^{-1/(1-\nu)}$, the boundary between I and III is $|\eta^*_{\text{sp}}(\omega)| \approx N^{-3\nu/(2-3\nu)}(\tau_0\omega)^{-1/(2-3\nu)}$, and the boundary between III and IV is $|\eta^*_{\text{sp}}(\omega)| \approx N_{\text{e}}(1)$, which is constant independent of ω. For θ solvents, the boundary between I and III/IV is given by $|\eta^*_{\text{sp}}(\omega)| \approx \frac{1}{N^3}(\tau_0\omega)^{-2}$, and the boundary between III and IV is $|\eta^*_{\text{sp}}(\omega)| \approx N_{\text{e}}(1)^{9/5}(\tau_0\omega)^{2/5}$, which is an increasing function of ω.

Our objective is to estimate these three relaxation times ($\tau_\xi,\ \tau_{\text{e}},\ \tau_{\text{rep}}$) in entangled semi-dilute polymer solution. For this purpose, we measure $|\eta^*_{\text{sp}}(\omega)|$ for a broad range of ω ranging from dilute regime (II) to flow regime (I) by using micro-rheology and macro-rheology. Time-concentration superposition is used to achieve such a wide spectrum of $|\eta^*_{\text{sp}}(\omega)|$ to investigate the polymer concentration dependence of these relaxation times.

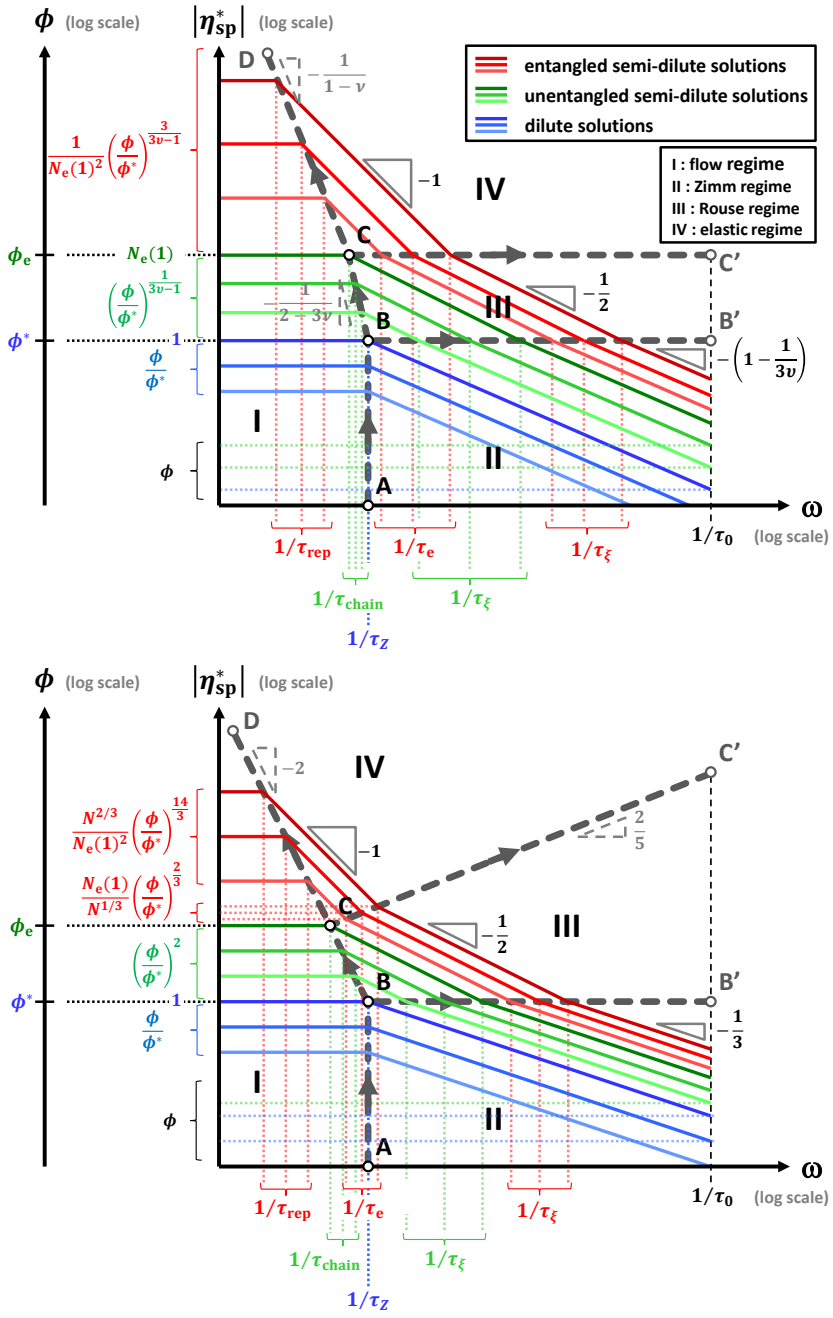

FIG. 1. (color online) Schematic representation of the magnitude of the complex specific viscosity $|\eta^*_{\rm sp}(\omega)| = |\eta^*(\omega) - \eta_{\rm s}|/\eta_{\rm s}$ for athermal solvents (top) and for θ solvents (bottom) as a function of frequency ω on log-log scale. In each figure, three blue lines represent $|\eta^*_{\rm sp}(\omega)|$ in dilute regime $\phi < \phi^*$, three green lines show $|\eta^*_{\rm sp}(\omega)|$ in unentangled semi-dilute regime $\phi^* < \phi < \phi_{\rm e}$, and three red lines represent $|\eta^*_{\rm sp}(\omega)|$ in entangled semi-dilute regime $\phi_{\rm e} < \phi \ll 1$. Gray dashed lines indicate boundaries of the dynamic regimes. I: flow regime, II: Zimm regime, III: Rouse regime, IV: elastic regime.

III. EXPERIMENTAL SECTION

A. Materials

Poly(ethylene oxide), PEO, (nominal molecular weight: 8000 kg/mol by supplier) was purchased from PolySciences. An aqueous suspension of polystyrene microspheres (stabilized with COOH groups at the surface) used as probe particles for DWS microrheology measurements were purchased from Micromod (Rostock, Germany). According to the supplier, the particle size is 500 nm. PEO aqueous solutions were prepared by dissolving PEO in Milli-Q water. Dissolution of PEO powders and homogenization of the PEO solutions were statically performed by osmotic pressure for 1 week without stirring the solutions so as to avoid chain scission. For DWS measurements, the polystyrene microspheres were also dispersed in the solution. The probe concentrations were 0.1, 0.25, or 1 % depending on PEO concentration.

B. Size characterization by light scattering

The size of the probe particles and the PEO polymer was characterized by light scattering with a 3-CGS ALV goniometer system. The hydrodynamic diameter of the probe particles in a dilute suspension (0.005 %) was determined by dynamic light scattering as $2R = 457$ nm. The hydrodynamic radius $R_{\rm h}$ of the PEO polymer extrapolated to infinite dilution was measured as 65 nm. The polydispersity index of the probe particles, defined as the square of the ratio of the standard deviation to the mean value, was measured to be less than 0.07, thus the particles can be considered as monodisperse. The polydispersity index of the PEO molecular weight was about 0.4, indicating that the polymer size is moderately polydisperse. The radius of gyration $R_{\rm g}$ was measured by static light scattering to be 160 nm. By assuming that the chain is Gaussian, the root-mean-square end-to-end distance in dilute solution, $R_{\rm Z}$, was estimated to be about 392 nm. By static light scattering, the molecular weight $M_{\rm w}$ (17000 kg/mol) and the second virial coefficient A_2 ($2.7 \times 10^{-11}{\rm m}^3{\rm mol/g}^2$) of PEO were also determined. The value of the intrinsic viscosity $[\eta]$ of the PEO in water

at 25 °C was estimated from the measured value of the molecular weight M_w by using the Mark-Houwink-Sakurada equation, $[\eta] = KM_w^{\alpha}$. Values of $[\eta]$ and M_w from two references [38, 39] were summarized to find the parameters K, α of the Mark-Houwink-Sakurada equation. We found $K = 0.050$ mL/g(mol/g)$^{\alpha}$ and $\alpha = 0.67$, thus $[\eta] = 3300$ mL/g for $M_w = 17000$ kg/mol. The overlapping concentration C^* is given by taking inverse of the intrinsic viscosity, as $C^* = 1/[\eta] = 3.0 \times 10^{-4}$ g/mL, or 0.03 %.

C. Classical macrorheology

A coaxial rotational viscometer (LS 400, Lamy Rheology, Lyon, France) with a cylindrical Couette geometry (length: 8 mm, inner diameter: 11 mm, outer diameter: 12 mm) was used to measure macroscopic flow behavior of the PEO solutions at different concentrations (0.005 - 0.15 %). For the concentrations between 0.2 and 2 %, a stress-controlled Haake RS600 rheometer with a cone-plate geometry (diameter: 35 mm, angle 2 $^{\circ}$, gap 103 μm) was used. Frequency sweep (between 0.001 and 100 rad/s) in small amplitude oscillatory shear measurements were performed with the RS600 rheometer for the PEO concentration ranging between 0.6 and 2 %. All the macroscopic rheological measurements were performed at 25 °C.

D. Microrheology

a. DWS microrheology Microrheological measurements based on diffusing-wave spectroscopy (DWS) were conducted using a laboratory-made setup. A Spectra-Physics Cyan CDRH laser, operating at the wave length $\lambda = 488$ nm with an output power of 50 mW, was used as coherent light source. The laser beam was expanded to approximately 1 cm in diameter with a beam expander. A plastic cuvette for spectroscopy (thickness $L = 4$ mm) was placed in a thermostated sample holder. The scattered light was collected by an optical fiber placed in the transmission geometry connected to a photon counter. Signals were treated by a digital correlator (ALV-7004/USB-FAST, ALV, Lanssen, Germany) to obtain an intensity autocorrelation function.

The obtained intensity autocorrelation function $g^{(2)}(t)$ was converted into the field autocorrelation function $g^{(1)}(t)$ by the Siegert relation, $g^{(2)}(t) = 1 + \beta[g^{(1)}(t)]^2$, then the MSD of the probe particles $\langle \Delta r_{\rm b}^2(t) \rangle_{\rm eq}$ was calculated by solving numerically the following equations [40, 41] for transmission geometry:

$$g^{(1)}(t) = \frac{\frac{L}{l^*} + \frac{4}{3}}{\frac{z_0}{l^*} + \frac{2}{3}} \frac{\sinh\left[\frac{z_0}{l^*}\tilde{r}(t)\right] + \frac{2}{3}\tilde{r}(t)\cosh\left[\frac{z_0}{l^*}\tilde{r}(t)\right]}{\left(1 + \frac{4}{9}\tilde{r}(t)^2\right)\sinh\left[\frac{L}{l^*}\tilde{r}(t)\right] + \frac{2}{3}\tilde{r}(t)\cosh\left[\frac{L}{l^*}\tilde{r}(t)\right]}, \tag{14}$$

where $\tilde{r}(t) \equiv \sqrt{(2\pi/\lambda)^2 \langle \Delta r_{\rm b}(t)^2 \rangle_{\rm eq}}$ is the root of the MSD nondimensionalized by the wave length, l^* is the sample transport mean free path of the scattered light determined from the values of transmission intensity of the sample and a reference sample (water) whose l^* is known. For this system l^* was found to be 1900, 670 and 190 μm for the probe concentrations of 0.1, 0.25 and 1 %, respectively. z_0 is the distance the light travels through the sample before becoming randomized, here it is set $z_0 = l^*$. The measured multiply scattered light signal was found to be ergodic for all the sample studied. With the experimental setup used, we can measure accurately the value of MSD up to about 400 nm^2. Thus the probe particles measure the length scale ($\sqrt{400\ \text{nm}^2} = 20$ nm) much smaller than the size of the particles (457 nm in diameter).

b. MSD analysis The dynamic modulus of the solution was estimated from the MSD of the probe particles by using the generalized Stokes-Einstein relation (GSER) [1]

$$G^*(\omega) = \frac{k_{\rm B}T}{\pi R i\omega \overline{\mathfrak{F}}\left\{\langle \Delta r_{\rm b}^2(t) \rangle_{\rm eq}\right\}} \tag{15}$$

where $\overline{\mathfrak{F}}\{\cdots\}$ indicates the one-sided Fourier transform. We study the frequency regime where inertial effects of the probe particles and solution are ineffective ($\omega \lesssim 10^6$ rad/s), so that we use the inertia-less GSER given by Eq. (15) rather than the inertial one [42, 43]. In usual passive microrheological analysis, MSD curve is fitted by a smooth function of time to transform it to that in the frequency domain (alternative method without fitting was also proposed [44, 45]). For this purpose, we used the fitting function that can be analytically transformed to obtain $G'(\omega)$ and $G''(\omega)$ by using special functions [46, 47]. In the rest of this paper, we abbreviate $\langle \Delta r_{\rm b}^2(t) \rangle_{\rm eq}$ as MSD(t) for simplicity.

IV. RESULTS AND DISCUSSION

A. Specific viscosity

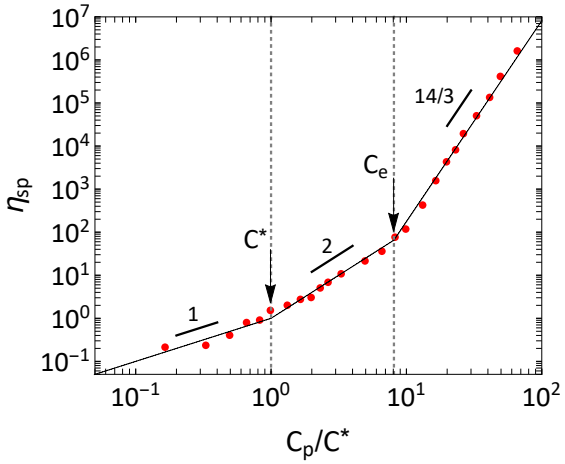

FIG. 2. Specific viscosity of PEO aqueous solution measured by macrorheology as a function of PEO concentration C_p. The overlap concentration is $C^* = 0.030$ %, and the entanglement concentration is $C_\mathrm{e} = 0.25$ %.

Figure 2 shows macro-rheologically measured specific viscosity $\eta_\mathrm{sp} = (\eta - \eta_\mathrm{s})/\eta_\mathrm{s}$ of PEO aqueous solutions as a function of the PEO concentration C_p normalized by the overlapping concentration C^*. η is the viscosity of PEO solution and η_s is the viscosity of water (0.89 mPas). We observe that η_sp exhibits typical scaling behaviors with three regimes. In dilute solution regime where $\eta_\mathrm{sp} < 1$, the values of η_sp are approximately equal to C_p/C^*. We can see from Fig. 2 that $\eta_\mathrm{sp} \approx 1$ at $C_\mathrm{p} = C^*$. At the polymer concentration higher than C^*, there is the unentangled semi-dilute regime, where we find $\eta_\mathrm{sp} \approx (C_\mathrm{p}/C^*)^2$. At further higher concentration in the entangled semi-dilute regime, the specific viscosity increases more sharply as $\eta_\mathrm{sp} \sim (C_\mathrm{p}/C^*)^{14/3}$. The entanglement concentration C_e is determined as a cross-over concentration between the unentangled regime ($C^* < C_\mathrm{p} < C_\mathrm{e}$) and entangled semi-dilute regime ($C_\mathrm{e} < C_\mathrm{p}$) as $C_\mathrm{e} \approx 0.25$ % (see Fig. 2).

The power-law behavior of η_sp as a function of C_p in the three concentration regimes

corresponds well to that expected for the polymer solutions in θ condition. The same behavior was demonstrated in the literature for PEO having $M_{\mathrm{w}} = 5000$ kg/mol (Fig. 8.11 in [34]). However, the exponent α of the Mark-Houwink-Sakurada equation from the literature is about 0.67 (see Figure S1) [38, 39], suggesting that water is a moderately good solvent of PEO. On the other hand, it might be noteworthy that the value of the second virial coefficient A_2 (thus the solvent quality) decreases with increase in the molecular weight [39]. For the PEO studied in this work, we found a positive value of A_2 but its absolute value is low ($A_2 = 2.7 \times 10^{-11} \mathrm{m}^3$ mol/g^2). The fact that the value of A_2 is small is consistent with our experimental result for η_{sp} indicating that the solution is in the θ condition.

B. Low-frequency behavior (macro-rheology)

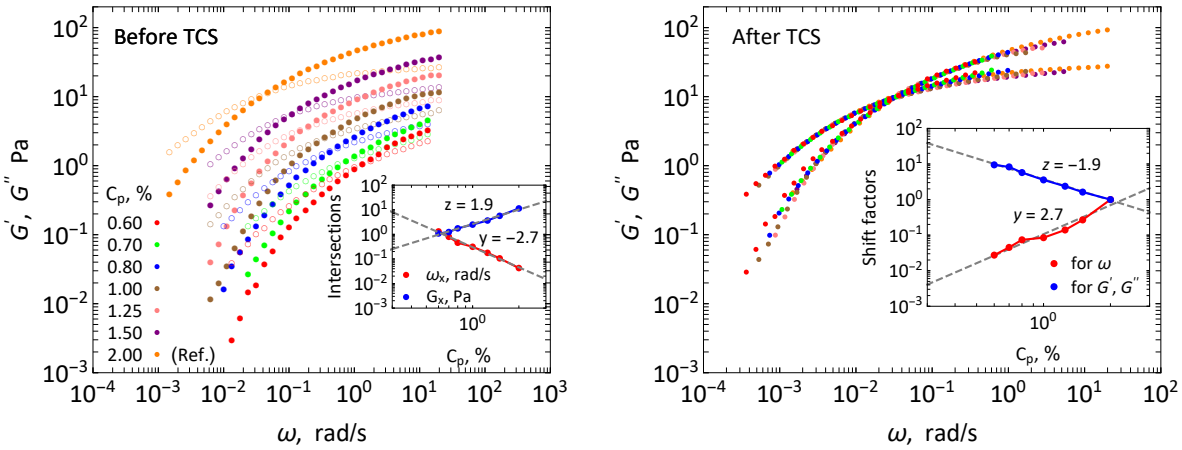

FIG. 3. (color online) Left: Macro-rheologically measured dynamic moduli of PEO aqueous solutions for several different polymer concentrations $C_{\rm p}$. Inset of left panel: Intersections $(\omega_{\rm x}, G_{\rm x})$ of $G'(\omega)$ and $G''(\omega)$ as a function of polymer concentration. Right: Master curve of the dynamic moduli made from individual curves shown in left panel. Reference polymer concentration is $C_{\rm p} = 2.0$ %. Inset of right panel: Horizontal shift factor (red) and vertical shift factor (blue) used to construct the master curve of the dynamic moduli.

In Fig. 3 left, the dynamic moduli of the PEO solutions in the entangled semi-dilute regime are shown as a function of the frequency, measured by macroscopic rheometry. In this frequency range, the viscoelastic response represented by the crossover between the storage modulus $G'(\omega)$ and loss modulus $G''(\omega)$ is observed. With increase in the PEO concentration, the crossover frequency decreases and the modulus increases, corresponding to the increase in the zero shear viscosity shown in Fig. 2. The concentration dependence of the dynamic moduli near terminal zone can be accurately studied by characterizing the crossing of G' and G'' at low frequency domain. In the inset of Fig. 3 left, the values of moduli, $G_{\rm x}$, and of frequency, $\omega_{\rm x}$, are plotted as a function of PEO concentration $C_{\rm p}$. We found power-law behavior as $\sim C_{\rm p}^{y}$ with $y = -2.7$ for $\omega_{\rm x}$, and $\sim C_{\rm p}^{z}$ with $z = 1.9$ for $G_{\rm x}$.

In order to check these results, we also performed time-concentration superposition (TCS)

to these curves of $G''(\omega)$ at terminal zone. In Fig. 3 right, master curve with the solution of $C_{\rm p} = 2.0$ % as reference is shown. The superposition is successfully performed, the whole frequency range measured here can be well superposed. At the higher frequency than the crossover point, $G'(\omega)$ is higher than $G''(\omega)$, corresponding to the transient elasticity by entanglements. At the lower frequency, $G''(\omega)$ is higher than $G'(\omega)$, corresponding to the terminal flow. In the inset of Fig. 3 right, the horizontal and vertical shift factors are plotted as a function of the PEO concentration. The horizontal shift factor (red) for ω scales with the PEO concentration as $\sim C_{\rm p}^{y}$ with $y = 2.7$, while the vertical shift factor (blue) for the modulus scales as $\sim C_{\rm p}^{z}$ with $z = -1.9$. These results are consistent with those obtained from $\omega_{\rm x}$ and $G_{\rm x}$.

According to Eq. (6) and Eq. (8), concentration dependence of the reptation time and the elastic plateau are $\tau_{\rm rep} \sim C_{\rm p}^{y}$ with $y = 3(1-\nu)/(3\nu-1)$ and $G_{\rm e} \sim C_{\rm p}^{z}$ with $z = 3\nu/(3\nu-1)$, respectively. Theoretically, we have $y = 1.6$ and $z = 2.3$ for a good solvent, $y = 2.3$ and $z = 2.3$ for a θ solvent. Experimentally, we found $y = 2.7$ and $z = 1.9$ from the terminal intersection ($\omega_{\rm x},\ G_{\rm x}$) between $G'(\omega)$ and $G''(\omega)$, which are consistent with the TCS's result. It should be noted that the experimental values of the power-law exponents ($y = 2.7,\ z = 1.9$) slightly different from the theoretical values for a θ solvent ($y = 2.3,\ z = 2.3$). For macro-rheology, similar discrepancy has been reported. Daga and Wagner found $y = 4.2 \pm 0.2$ and $z = 0.72 \pm 0.08$ for PEO in water [27]. Baumgartel et al. found similar values with ours, $y = 3.5 \pm 0.2$ and $z = 2.2 \pm 0.2$ for polystyrene in ethylbenzene [31]. Experimental results and literature values are summarized in Table I. In this system, a well defined elastic plateau due to the entanglements is not observed, presumably due to the polydispersity of the PEO used. We do not further discuss this point as it is not the main purpose of this work.

	this work		Ref.[27]	Ref.[31]	theory
polymer	poly(ethylene oxide)		poly(ethylene oxide)	polystyrene	–
solvent	water		water	ethylbenzene	apolar ($\nu = 0.588$)
molecular weight (kg/mol)	8000 (nominal) 17000 (measured)	900	247 and 374	–	–
concentration	0.05–2 %		2.24–6.5 %	40.6–100 %	–
method	micro-rheology	macro-rheology	macro-rheology	macro-rheology	–
$\lvert y \rvert$ $(\tau_\xi, \tau_\mathrm{e})$	2.6	–	–	–	$\frac{3\nu}{3\nu-1} = 2.3$
z (G_ξ, G_e)	2.5	–	–	–	$\frac{3\nu}{3\nu-1} = 2.3$
y (τ_rep)	–	2.7	4.2 ± 0.2	3.5 ± 0.2	$\frac{3(1-\nu)}{3\nu-1} = 1.6$
z (G_e)	–	1.9	0.72 ± 0.08	2.2 ± 0.2	$\frac{3\nu}{3\nu-1} = 2.3$

TABLE I. Absolute values of the exponents y, z for the relaxation time and the modulus (or MSD), respectively.

C. Comparison between macro- and micro-rheology

In order to figure out the accessible ranges in time (or frequency) and MSD (or dynamic modulus/complex viscosity), and also in order to validate the accuracy of the microrheological measurements, DWS microrheology were performed by using three different probe concentrations, and the results are compared with those from macro-rheology. In Fig. 4 left, the values of MSD for $C_\mathrm{p} = 0.7$ % measured with three different probe concentrations are shown. The corresponding data for $C_\mathrm{p} = 0$ % (thus solvent, water) are also plotted as a reference. The results for the three probe concentrations overlap well on each other, covering a wide range in time ($10^{-6} \lesssim t \lesssim 10^2$ s) and in MSD ($10 \lesssim$ MSD $\lesssim 10^5$ nm^2). For the solvent, we find MSD$(t) \propto t^1$ at the whole time scale, as expected for a Newtonian fluid. For the PEO solution at $C_\mathrm{p} = 0.7$ %, MSD shows an anomalous but typical time dependence for a viscoelastic polymer solution. Starting from the high frequency range, where the values of MSD are close to but lower than those in water, the power-law exponent β in MSD$(t) \propto t^\beta$ gradually decreases with increase in time. After an inflection point at about $t \approx 0.01$ s, β restarts to increase, approaching to 1. With increase in the probe concentration, the value

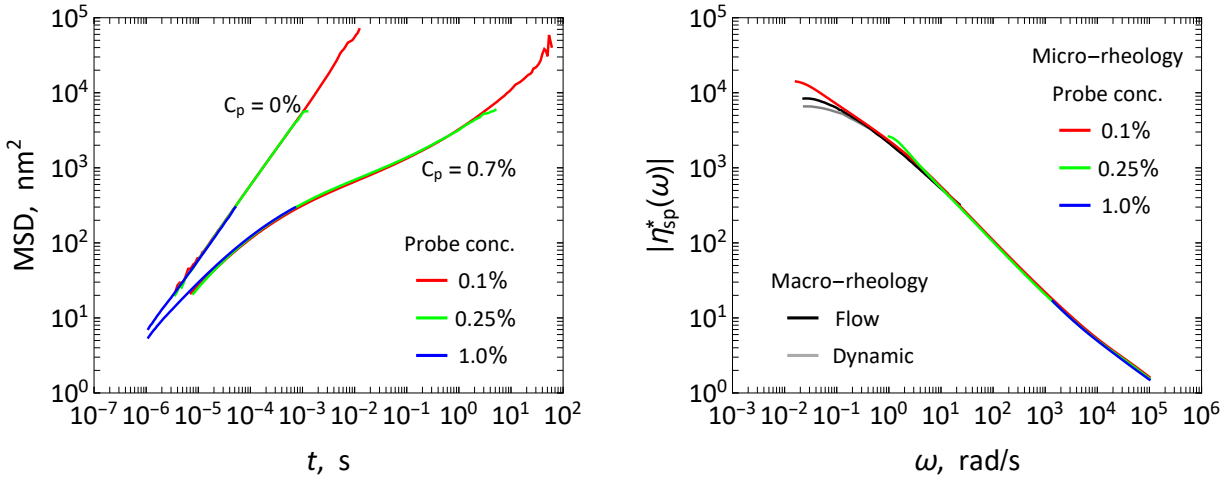

FIG. 4. (color online) Left: Mean-square displacement (MSD) of probe particles dispersed in water (C_p = 0 %) and in PEO aqueous solution (C_p = 0.7 % [C_p/C^* = 23]) for three probe concentrations as a function of time. Right: Absolute value of the complex specific viscosity of PEO aqueous solution (C_p = 0.7 %). Red, green and blue lines: micro-rheology using 0.1 % (red), 0.25 % (green) and 1.0 % (blue) probe concentrations. Black line: macro-rheology by flow test. Gray line: macro-rheology by dynamic test.

of sample transport mean free path l^* decreases, and accessible MSD range shifts to lower values. At the given experimental conditions, with the probe concentration of 1 %, the smaller limit of MSD can be as low as several nm^2, giving an advantage of the method. It is possible to expand the accessible time range to longer time scale by decreasing the probe concentration.

A simple way to validate the accuracy of micro-rheology is to compare it with macro-rheology. Since we can reasonably consider that the probe size ($2R$ = 457 nm) is sufficiently larger than the characteristic length scales of the polymer solutions, the GSER can be applied to estimate rheological properties of the solution from MSD of the probes dispersed in the solution. From MSD, complex modulus then complex viscosity are calculated with the help of the GSER. In Fig. 4 right, absolute value of the micro-rheologically determined complex specific viscosity is plotted as a function of frequency for the three probe concentrations, compared with that from macro-rheology in both flow and dynamic measurements. We can

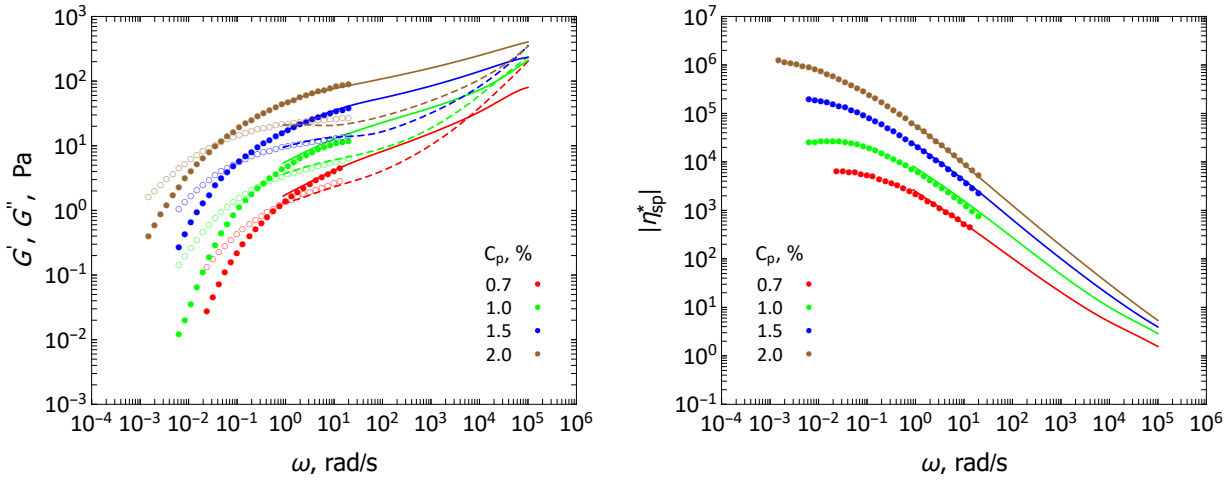

FIG. 5. (color online) Left: Dynamic moduli of PEO aqueous solutions. Solid (or dashed) lines: storage (or loss) modulus by micro-rheology. Closed (or open) circles: storage (or loss) modulus by macro-rheology. Polymer concentrations are 0.7 % (red), 1.0 % (green), 1.5 % (blue), and 2.0 % (brown). Right: Absolute value of the complex specific viscosity of PEO aqueous solution. Solid lines: micro-rheology. Closed circles: macro-rheology. Probe concentration is 0.25 % for all polymer concentrations.

see that the three curves for micro-rheology and those for macro-rheology superpose with each other, covering a wide time range. This result indicates that the GSER can be applied to estimate the viscoelastic properties of this system.

In Fig. 5, macro- and micro-rheology are compared for four representative polymer concentrations in entangled concentration regime. Left panel shows the dynamic modulus $G^*(\omega)$. In macro-rheology which covers a frequency range of about $0.001 < \omega < 100$ rad/s, Maxwell-like behavior of entangled polymer solutions is observed. A crossover between $G'(\omega)$ and $G''(\omega)$ exists for all the polymer concentrations shown here. In the same figure, results of microrheology with a probe concentration of 0.25 % are also shown. We can access a frequency range of about $0.1 < \omega < 10^5$ rad/s by micro-rheology, partly overlapping the frequency range of macro-rheology. Right panel shows the absolute value of the complex

specific viscosity $\eta^*_{\rm sp}(\omega) = (\eta^*(\omega) - \eta_{\rm s})/\eta_{\rm s}$, where the complex viscosity $\eta^*(\omega) = G^*(\omega)/(i\omega)$ is derived from $G^*(\omega)$ shown in the left panel. We see that macro-rheological $G^*(\omega)$ and $|\eta^*_{\rm sp}(\omega)|$ agree well with those estimated by DWS micro-rheology without adjustable parameters at intermediate overlapping frequencies.

D. High-frequency behavior (micro-rheology)

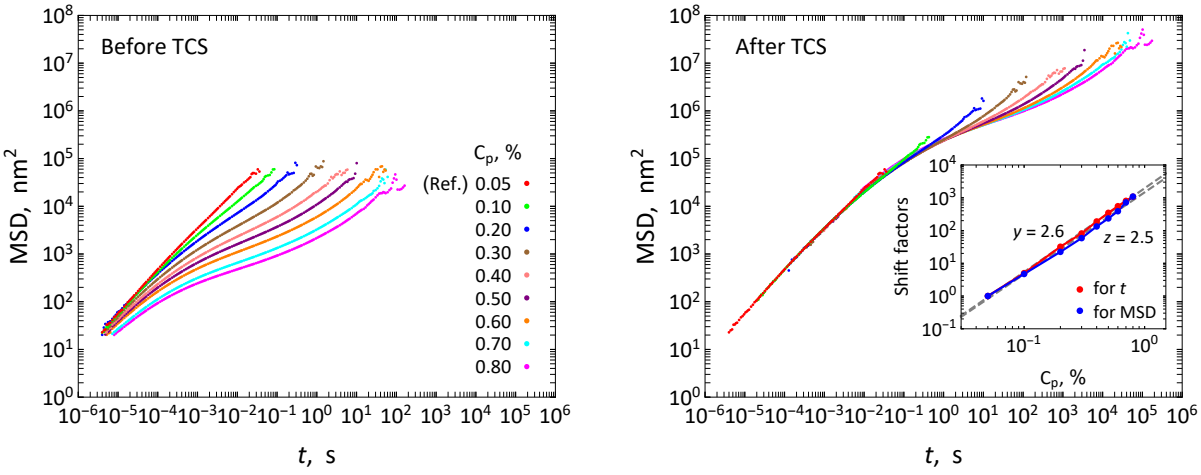

FIG. 6. (color online) Left: Mean-square-displacement (MSD) of probe particles dispersed in PEO aqueous solution for each polymer concentration before shifting the curves. Right: Master curve constructed at *short* time regime made from individual MSD curves shown in left panel. Reference polymer concentration is 0.05 %. Overlapping concentration is $C^* = 0.030$ %. Inset of right panel: Concentration dependence of the horizontal shift factor (red) and vertical shift factor (blue) used to construct the MSD master curve. Probe concentration is 0.1 % for all polymer concentrations.

As shown in Fig. 1, there should be the Rouse mode at the time scale shorter than the elastic plateau, and the boundary between these two modes should give the Rouse time τ_e of the ideal chain (of blobs) between two neighboring entanglements. To study the Rouse mode in more detail, it is rational to extend the polymer concentration range to the unentangled semi-dilute regime. Here we examine TCS for MSD for a polymer concentration range between 0.05 and 0.8 %, to superpose the data of MSD at short time scale. The probe concentration is 0.1 %. Corresponding macroscopic measurements cannot be performed as the short time range is not accessible with conventional mechanical rheometers. In Fig. 6 left, curves of the original MSD before performing TCS are shown. These data cover the short time range down to about 10^{-5} s, where polymer concentration dependence is weak. At long time range, more pronounced polymer concentration dependence appears, and the

values of MSD are lower for higher polymer concentrations, corresponding to the transient elasticity due to entanglements. Using the lowest polymer concentration studied here (0.05 %) as reference, we found that a TCS is satisfied for the short time range as shown in Fig. 6 right. As expected, the data at long time range are not superposed with this TCS. In the inset of Fig. 6 right, the vertical and horizontal shift factors are plotted as a function of the polymer concentration. The values of the vertical and horizontal shift factors exhibit power-law behavior, and they are almost identical to each other. That is, the horizontal shift factor (red) for t scales with the PEO concentration as $\sim C_{\rm p}^{y}$ with $y = 2.6$, and the vertical shift factor (blue) for MSD scales as $\sim C_{\rm p}^{z}$ with $z = 2.5$.

According to the theoretical predictions, for athermal solvents, relaxation time of entanglement strands and entanglement plateau modulus depend on the polymer volume fraction ϕ as $\tau_{\rm e} \sim \phi^{y}$ with $y = -3\nu/(3\nu - 1)$ and $G_{\rm e} \sim \phi^{z}$ with $z = 3\nu/(3\nu - 1)$ respectively (see Eqs. (5) and (8)). Thus, we have $|y| = z \simeq 2.3$. These values are similar to those which we experimentally found, 2.5 and 2.6. It should be noted that for θ solvents, $|y| = 5/3 \simeq 1.7$ and $z = 7/3 \simeq 2.3$. Thus we conclude that the entanglement time, the longest limit of the relaxation time of the Rouse mode, in a good solvent is successfully detected (see Table I).

E. Analysis of Rouse and Zimm modes

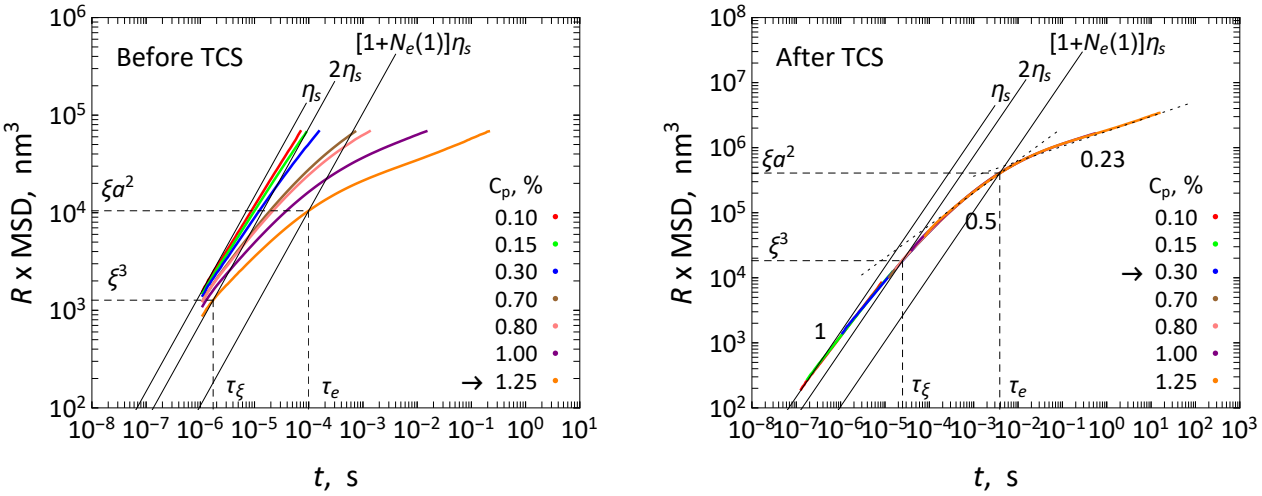

FIG. 7. (color online) Left: Time dependence of the product of the particle radius (R) and mean-square-displacement (MSD) of probe particles dispersed in PEO aqueous solutions. For $C_\mathrm{p} = 1.25\%$, we obtain $\tau_\mathrm{e} \approx 0.00010$ s, $\tau_\xi \approx 1.7 \times 10^{-6}$ s, $a \approx 31$ nm and $\xi \approx 11$ nm when $N_\mathrm{e}(1) = 13$ (see text). Right: Master curve constructed by shifting the original curves shown in left panel so that they overlap at *short* time regime. Reference polymer concentration is 0.3 %. We obtain $\tau_\mathrm{e} \approx 0.0039$ s, $\tau_\xi \approx 0.000025$ s, $a \approx 124$ nm and $\xi \approx 26$ nm. Probe concentration is 1 %.

As shown in the previous section (IV D), TCS at short time range allowed us to detect the Rouse mode. Here we further characterize the Rouse mode as quantitatively as possible by inspecting the upper and lower limits of it in the MSD curve. To improve further accuracy of the measurements for small values of MSD, we used the MSD data measured with the probe concentration of 1 %. Now it is beneficial to consider the product of MSD and the probe size R, as it has the unit of volume thus allows us to compare it with characteristic volumes of the system [48]. In Fig. 7 left, $R \times$ MSD is plotted as a function of time for various PEO concentrations. Here we propose a new method to evaluate the upper and lower limit of the Rouse mode.

The *upper* limits of $R \times$MSD and t of the Rouse regime correspond to the occupied volume

$a^2\xi$ and relaxation time $\tau_{\rm e}$ of the entanglement strand, respectively, and as shown in Eq. (11), the corresponding specific viscosity is $\eta_{\rm sp} \approx N_{\rm e}(1)$ (or solution viscosity $\eta \approx [1 + N_{\rm e}(1)]\eta_s$). According to the Stokes-Einstein law, the value of $R \times$ MSD for the purely viscous solution with the viscosity $[1 + N_{\rm e}(1)]\eta_s$ is given by $\frac{k_B T}{[1+N_{\rm e}(1)]\eta_s \pi} t$. By using the reference value of $N_{\rm e}(1) = 13$, we can plot it as a function of time in Fig. 7 left as a gray straight tilted line labeled as "$[1 + N_{\rm e}(1)]\eta_{\rm s}$". We assume that the vertical and horizontal coordinates of this cross-point give $R \times \mathrm{MSD} \approx a^2\xi$ and $t \approx \tau_{\rm e}$, respectively. As an example, in the figure, the crossover point for $C_{\rm p} = 1.25$ % is shown.

We apply the same argument to the *lower* limit of the Rouse regime. The lower limits of $R\times$MSD and t of the Rouse regime correspond to the occupied volume ξ^3 and relaxation time τ_ξ of the blob, respectively, and as shown in Eq. (11), the corresponding specific viscosity is $\eta_{\rm sp} \approx 1$ (or solution viscosity $\eta \approx 2\eta_{\rm s}$). The value of $R \times$ MSD ($= \frac{k_{\rm B}T}{2\eta_{\rm s}\pi} t$) corresponding to the viscosity $2\eta_{\rm s}$ is drawn in Fig. 7 left as a gray straight tilted line labeled as "$2\eta_{\rm s}$". We suppose that this cross-point indicates the *lower* limit of the Rouse regime thus its vertical and horizontal coordinates give $R \times \mathrm{MSD} \approx \xi^3$ and $t \approx \tau_\xi$, respectively. Consequently, we have $\tau_{\rm e} \approx 0.00010$ s, $\tau_\xi \approx 1.7 \times 10^{-6}$ s, $a \approx 31$ nm and $\xi \approx 11$ nm for the polymer concentration $C_{\rm p} = 1.25$ % (see Fig. 7 left). It should be noted, however, that the two cross-points exist only at the limited concentrations due to the narrow data range of $R \times$ MSD. For example, for the polymer concentration $C_{\rm p} = 1.25$ %, both upper and lower cross-points can be found, while for $C_{\rm p} = 0.3$ %, no upper cross-point can be detected.

In order to expand the data range, we used the TCS method. The master curve of $R\times$MSD was successfully obtained from the data shown in Fig. 7 left similarly to the result of MSD with the probe concentration of 0.1 % (Fig. 6). Reference polymer concentration to make the master curve is set to 0.3 % which is above $C_{\rm e}$. It is demonstrated that the master curve has both upper and lower cross-points with the lines corresponding to the solution viscosity of $2\eta_{\rm s}$ and $[1+N_{\rm e}(1)]\eta_s$. The slope of the master curve $\beta = d\ln \mathrm{MSD}(t)/d\ln t$ varies smoothly with time, while we can idenfity a regime with β about 0.23 at long-time range over several decades, corresponding to the elastic "plateau" by the entanglements. With decrease in time, β gradually increases, and at about $t = 0.01$ s, we see a regime where β

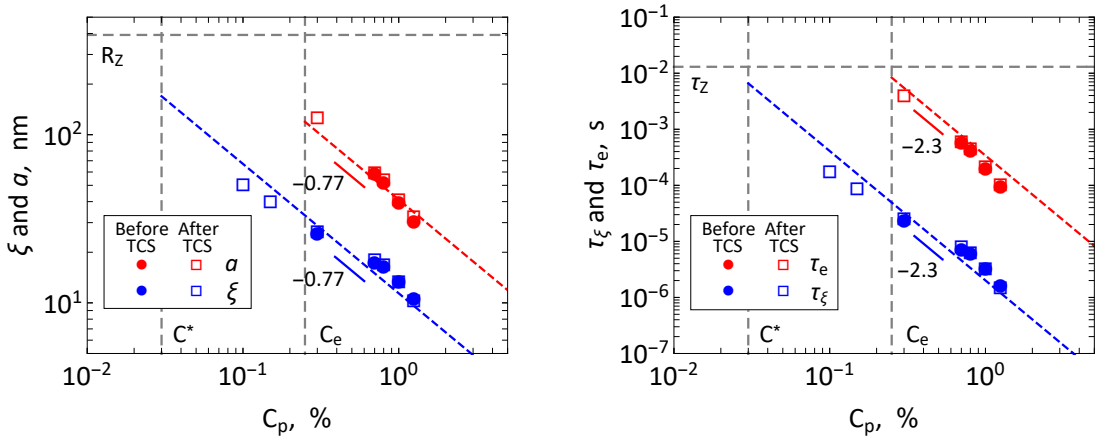

FIG. 8. (color online) Characteristic lengths ξ, a (left) and characteristic times τ_ξ, τ_e (right) as a function of polymer concentration on log-log scale. Filled circles show these quentities estimated from the original MSD curves before performing the TCS (Fig. 7 left), whereas open squares represent those obtained from the MSD master curve after the TCS (Fig. 7 right).

is about 0.5, corresponding to the Rouse mode. The upper cross-point seems close to the upper limit of this power-law regime, while the lower cross-point is slightly lower than the lower limit of this power-law regime. At further short time range, β increases to about 1, and the value of $R \times$ MSD is very close to that of the probe in the solvent (water) with the viscosity of η_s shown as gray line labeled as "η_s". Note that inertial effects that should exist at this short time regime ($\approx 10^{-7}$ s) cannot be detected in the TCS master curve because the master curve at this regime is just an extrapolation of the curves at longer time regime where inertial effects do not exist.

The reference polymer concentration to make the TCS master curve can be arbitrarily chosen. For each reference concentration, a set of the four parameters (ξ, a, τ_ξ, τ_e) can be determined by the same method as explained in the previous paragraph for the original curves without the TCS. Figure 8 shows log-log plots of the thus-obtained ξ and a versus C_p (left panel) as well as τ_ξ and τ_e versus C_p (right panel) by open symbols. The same set of data, determined from the original $R \times$ MSD curves without the TCS (Fig. 7 left), is also plotted in Fig. 8. The two data sets are sufficiently close and TCS can provide more data points at lower concentrations.

As seen in Fig. 8 left, both ξ and a decrease with increasing C_p, exhibiting a power-

law behavior. Since the theory predicts $\xi \approx b\phi^{-\nu/(3\nu-1)}$ (Eq. (1)), we fitted the data of ξ, obtained from the TCS master curve, by Eq. (1) with b as a fitting parameter. With the reference value $\nu = 0.588$, the power-law fit (blue dashed line) is well performed, and we found $b = 0.81$ nm [49]. The order of this value is sound, compared to the reference values (1.1 nm for a melt [34], 0.7 nm measured by single molecule force spectroscopy by atomic force microscopy for aqueous solution [50]). The tube diameter a is proportional to ξ, i.e., $a \approx \xi\sqrt{N_{\rm e}(1)} \approx b\sqrt{N_{\rm e}(1)}\phi^{-\nu/(3\nu-1)}$ for athermal solvents, thus both lengths exhibit the same power-law exponent. With the result of the fit for ξ and with the reference value of $N_{\rm e}(1) = 13$, we can also draw a prediction line for a for athermal solvents (red dashed line in Fig. 8 left). We see that the predicted power-law exponent is found reasonably close to experimental one.

It is worth comparing these characteristic lengths ξ and a with the polymer size $R_{\rm Z} \approx$ 392 nm in dilute solution, which is indicated by a dashed horizontal line in Fig. 8 left. By extrapolating the experimental values of ξ to lower concentration domain (dashed blue line in Fig. 8 left), we find that the extrapolated ξ at C^* is roughly close to $R_{\rm Z}$, as expected from theory. Also, theory predicts that $R_{\rm Z}$ is close to a at $C_{\rm p} = C_{\rm e}$ [34], which is also roughly confirmed in the same figure. These results suggest validity of the estimated ξ and a by the method proposed here.

In the right panel of Fig. 8, the values of τ_ξ and τ_e are plotted as a function of $C_{\rm p}$. These two characteristic time decrease with increasing the polymer concentration, exhibiting a power-law behavior. We fitted the data of τ_ξ with Eq. (4), $\tau_\xi \approx \tau_0\phi^{-3\nu/(3\nu-1)}$, by using $\nu = 0.588$ to find the value of τ_0. The blue dashed line with $\tau_0 = 0.73$ ns fits well with the experimental result obtained from the TCS master curve [51]. Equation (5) indicates $\tau_{\rm e} \approx N_{\rm e}(1)^2\tau_\xi \approx \tau_0 N_{\rm e}(1)^2\phi^{-3\nu/(3\nu-1)}$ for athermal solvents, allowing us to draw the corresponding theoretical value of $\tau_{\rm e}$ (red dashed line in Fig. 8 right). This line well superposes on the experimental values of $\tau_{\rm e}$. We can also estimate τ_0 from b by using $\tau_0 \approx \frac{\eta_{\rm s}b^3}{k_{\rm B}T}$ (Eq. (3)). With $b = 0.81$ nm determined from the fitting of ξ, we found $\tau_0 = 0.12$ ns. This value is smaller than but comparable to that determined from the fitting of τ_ξ. By using the value of the polymer size in dilute solution $R_{\rm Z}$ (≈ 392 nm), the characteristic relaxation time of the

polymer, $\tau_{\rm Z}$, can be estimated as $\tau_{\rm Z} \approx \frac{\eta_{\rm s} {R_{\rm Z}}^3}{k_{\rm B}T} \approx 0.013$ s. This value is close to τ_ξ extrapolated to $C_p = C^*$ (blue dashed line) as theoretically predicted. These results confirm that the high-frequency TCS can observe the scaling behavior of the characteristic times related to the Rouse mode reasonably well.

At further shorter time scale, there is a transition of the dynamic modes, from Rouse mode to Zimm mode. This crossover point is determined by the blob size ξ, with its characteristic relaxation time τ_ξ and modulus G_ξ. Thus Zimm mode is expected to be found in the narrow zone between the tilted line of $R \times$ MSD for $\eta_{\rm s}$ and that for $2\eta_{\rm s}$. However, it is difficult to investigate the power-law behavior of the Zimm mode in this narrow range, since the effect of the solvent cannot be easily removed from MSD.

In order to observe the Zimm mode, we switch to the complex viscosity, since the contribution of the solvent can be removed from it in a straightforward way when it is expressed as the specific viscosity, and on log-log scale the regime corresponding to the Zimm mode is expanded (regime II in Fig. 1). Figure 9 left shows the magnitude of the microrheological complex specific viscosity $|\eta^*_{\rm sp}(\omega)|$ before performing the TCS derived from the MSD shown in Fig. 7 left by using GSER for each polymer concentration. As we explained in Fig. 1, the upper and lower limits of the Rouse regime are given by $|\eta^*_{\rm sp}(\omega)| \approx N_{\rm e}(1)$ and $|\eta^*_{\rm sp}(\omega)| \approx 1$. They are indicated as horizontal black solid lines in Fig. 9 left. The cross-point between the horizontal line for $|\eta^*_{\rm sp}(\omega)| \approx N_{\rm e}(1)$ and the curves for $|\eta^*_{\rm sp}(\omega)|$ should correspond to $1/\tau_{\rm e}$. In the figure, as an example, the cross-point for the polymer concentration $C_{\rm p} = 0.8$ % is shown. We found $\tau_{\rm e} = 0.00038$ s. In the same manner, the cross-point with the horizontal line $|\eta^*_{\rm sp}(\omega)| \approx 1$ can be used to determine τ_ξ, and the cross-point for $C_{\rm p} = 0.3$ % is shown in the figure (we found $\tau_\xi = 0.000015$ s).

It should be noted that these cross-points can be observed only for a limited range of concentration because frequency range of the measurable $|\eta^*_{\rm sp}(\omega)|$ is restricted due to measurement limit of the MSD. It is thus useful to apply the TCS to expand the accessible frequency range of $|\eta^*_{\rm sp}(\omega)|$. Figure 9 right shows the master curve of $|\eta^*_{\rm sp}(\omega)|$ with $C_{\rm p} = 0.3$ % as a reference concentration. The shift factors to make the master curve are shown in Fig. 10 left. Both vertical (for $|\eta^*_{\rm sp}|$) and horizontal (for ω) shift factors exhibit power-law behaviors.

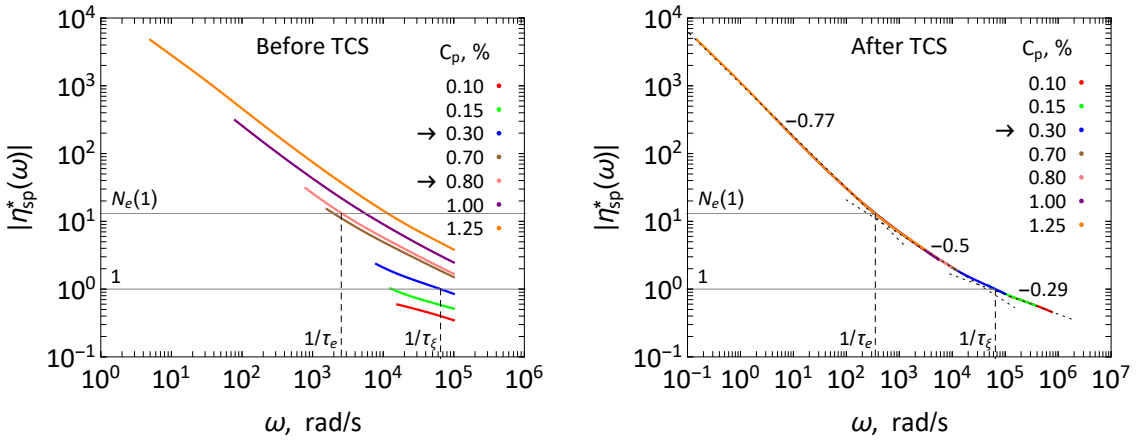

FIG. 9. (color online) Left: Micro-rheological absolute specific viscosity $|\eta^*_{\rm sp}(\omega)|$ for PEO aqueous solutions. Polymer concentration $C_{\rm p}$ is different for each curve. We obtain $\tau_\xi = 0.000015$ s for $C_{\rm p} = 0.3\%$ and $\tau_{\rm e} = 0.00038$ s for $C_{\rm p} = 0.8\%$. Right: Master curve of $|\eta^*_{\rm sp}(\omega)|$ constructed by shifting the original curves shown in the left panel. Reference polymer concentration is 0.3 %. We obtain $\tau_{\rm e} = 0.0028$ s and $\tau_\xi = 0.000015$ s for this reference polymer concentration (0.3%). Probe concentration is 1%.

We found that the exponent of the vertical shift factor is -0.033, and that of the horizontal shift factor is -2.2. These values well agree with the theoretical values for the Rouse mode (and the Zimm mode) in a good solvent, i.e., 0 for $|\eta^*_{\rm sp}|$ and -2.3 for $\tau_{\rm e}$ (and τ_ξ) (see Eqs. (4), (5) and (11)).

We can see from Fig. 9 right that the superposition of $|\eta^*_{\rm sp}(\omega)|$ is satisfactory, covering a wide range of the specific viscosity and frequency. The cross-points of the master curve with the horizontal lines $|\eta^*_{\rm sp}(\omega)| \approx N_{\rm e}(1)$ and $|\eta^*_{\rm sp}(\omega)| \approx 1$ exist, and between them, a power-law behavior with a slope of -0.5 is observed. Thus this mode well corresponds to the Rouse mode (see regime III in Fig. 1 top). ¿From the cross-points, we found $\tau_{\rm e} = 0.0028$ s and $\tau_\xi = 0.000015$ s when the reference concentration is 0.3 %. These values are close to those determined from the MSD master curve (0.0039 s and 0.000025 s) shown in Fig. 7 right. Furthermore, the ratio between $\tau_{\rm e}$ and τ_ξ is $\tau_{\rm e}/\tau_\xi \approx 187$, which is close to $N_{\rm e}(1)^2 = 13^2 = 169$. These results confirm the presence of the Rouse mode at $1/\tau_{\rm e} < \omega < 1/\tau_\xi$.

In Fig. 10 right, we compared the values of $\tau_{\rm e}$ and τ_ξ determined from MSD and $|\eta^*_{\rm sp}|$, before and after performing the TCS for these quantities. Similarly to the results for MSD

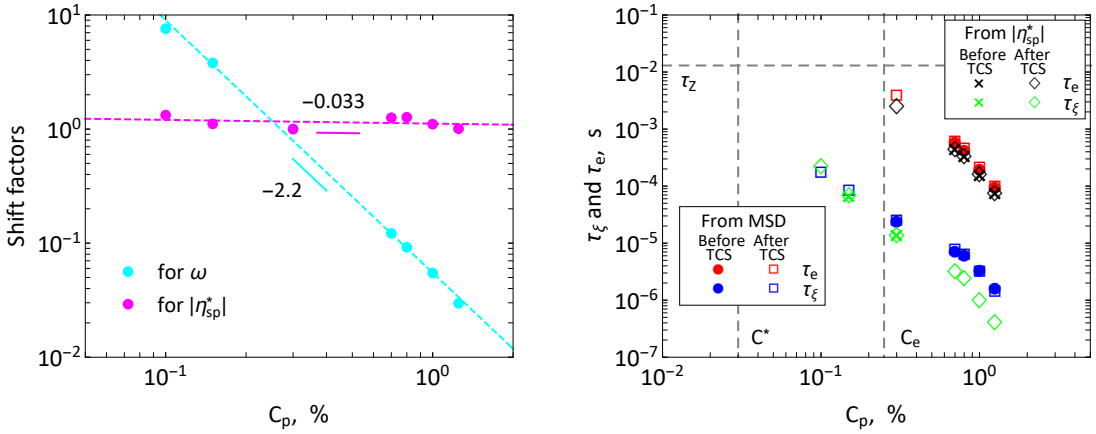

FIG. 10. (color online) Left: Horizontal shift factor (cyan) and vertical shift factor (magenta) that were used to construct the master curve of $|\eta^*_{\rm sp}(\omega)|$ shown in Fig. 9 right. Right: Diagonal crosses ($\times$) represent τ_ξ and $\tau_{\rm e}$ estimated from the original $|\eta^*_{\rm sp}(\omega)|$ curves before performing the TCS (Fig. 9 left), whereas the open diamonds ($\diamond$) show τ_ξ and $\tau_{\rm e}$ derived from the master curve of $|\eta^*_{\rm sp}(\omega)|$ after the TCS (Fig. 9 right). The remaining data (filled circles and open squares) are the same as those presented in Fig. 8 right.

shown in Fig. 8 right, the TCS for $|\eta^*_{\rm sp}(\omega)|$ allows us to have more data points (especially those of τ_ξ) than before performing the TCS. The results from MSD and those from $|\eta^*_{\rm sp}(\omega)|$ are very close, suggesting that the method applying the cross-points with the auxiliary lines is valid.

In a wide range at low frequency covering about 10^{-1} rad/s $< \omega < 10^2$ rad/s, a power-law behavior with a slope of -0.77 is found (Fig. 9 right), which should correspond to the elastic "plateau" (regime IV in Fig. 1 top), though the value of the slope is different from that expected from theory (-1). At the high frequency range, another dynamic mode is recognized because the power-law exponent changes from -0.5 to about -0.29. The crossover between this new mode and the Rouse mode is observed where $|\eta^*_{\rm sp}(\omega)| \approx 1$ (see the horizontal line connecting points B and B' in Fig. 1). Therefore we believe that the Zimm mode is observed in $|\eta^*_{\rm sp}(\omega)|$ at frequencies higher than $1/\tau_\xi$ corresponding to $|\eta^*_{\rm sp}(\omega)|$ smaller than 1, though the value of the slope in this range, -0.29, is slightly different from the theoretical value of the slope for the Zimm mode, -0.43 (with $\nu = 0.588$). This discrepancy is not due to the TCS. As shown in Fig. 9 right, though the data range is limited, still one can see that the curves for $C_{\rm p} = 0.10$ and 0.15 % before the TCS exhibit already the

slope of -0.29. There are several possible reasons for this discrepancy. Firstly, at the high frequency domain satisfying $|\eta^*_{\rm sp}(\omega)| \lesssim 1$, where $|\eta^*(\omega)|$ of the solution is comparable to the solvent viscosity $\eta_{\rm s}$, subtraction of $\eta_{\rm s}$ from $|\eta^*(\omega)|$ enlarges errors in $|\eta^*_{\rm sp}(\omega)|$. Secondly, error in the measurement of the particle size (a few %) propagates to the microrheological $|\eta^*_{\rm sp}(\omega)|$ through GSER, which is enlarged at high frequency because the value of the real part of the complex viscosity $\eta'(\omega)$ becomes close to the solvent viscosity $\eta_{\rm s}$.

V. CONCLUSION

We studied linear viscoelasticity of high molecular-weight linear flexible polymer in semi-dilute entangled concentration regime by using passive microrheology based on diffusing-wave spectroscopy (DWS). We successfully detected the Rouse regime for a chain of blobs where the frequency-dependence of $|\eta^*_{\rm sp}(\omega)|$ is $\approx \omega^{-1/2}$ at $1/\tau_{\rm e} < \omega < 1/\tau_\xi$ and the time-dependence of the mean-square displacement (MSD) is $\approx t^{1/2}$ at $\tau_\xi < t < \tau_{\rm e}$. We confirmed that both lower bound ($t = \tau_\xi$) and upper bound ($t = \tau_{\rm e}$) of the Rouse regime show the power-law behavior predicted by the theory. The values of the crossover times $\tau_{\rm e}$ and τ_ξ estimated from $|\eta^*_{\rm sp}|$ well agreed with those estimated from $R \times$ MSD with and without the time-concentration superposition. Considering that the upper bound of the Zimm regime corresponds to the lower bound of the Rouse regime, we can conclude that the upper bound of the Zimm mode at $t = \tau_\xi$ was successfully detected by the DWS microrheology too. To the best of the authors' knowledge, this is the first systematic microrheological observation of the crossover of these two modes characterized by the blob.

At $t < \tau_\xi$, Brownian motion of the probe particles in polymer solution is dictated by the viscosity of solvent. But there seems to be no reasonable way (so far) to subtract the contribution from the solvent viscosity $\frac{k_{\rm B}T}{\pi R \eta_{\rm s}} t$ from the MSD of the particles in the solution. Thus it would be hard to detect the characteristic power-law behavior of the Zimm mode in the MSD that should exist at $t < \tau_\xi$. On the other hand, in the microrheological $|\eta^*_{\rm sp}(\omega)|$, solvent viscosity $\eta_{\rm s}$ is already subtracted from the complex viscosity $\eta^*(\omega)$. Thus it would be natural to expect that the microrheological $|\eta^*_{\rm sp}(\omega)|$ could detect the Zimm mode at $\omega > 1/\tau_\xi$

where the effect of the solution viscosity is nonnegligible. We observed $|\eta^*_{\rm sp}(\omega)| \approx \omega^{-0.29}$ at $\omega > 1/\tau_\xi$, which is slightly different from the one expected from the theory ($\approx \omega^{-0.43}$). The discrepancy may be attributed to dispersity of the particle size that fluctuates a few % around its average because error in the microrheological $|\eta^*_{\rm sp}(\omega)|$ is more influenced by the particle size at higher frequency. A systematic study for the effect of particle size on viscoelastic functions in high-frequency regime and MSD of probe particles in short time regime is a future work.

VI. AUTHOR DECLARATIONS

Conflict of Interest The authors have no conflicts to disclose.

VII. DATA AVAILABILITY

The data presented in this study are available on request from the corresponding authors.

---

[1] T. G. Mason and D. A. Weitz, "Optical measurements of frequency-dependent linear viscoelastic moduli of complex fluids," Physical Review Letters, vol. 74, pp. 1250–1253, 1995.

[2] T. G. Mason, K. Ganesan, J. H. van Zanten, D. Wirtz, and S. C. Kuo, "Particle tracking microrheology of complex fluids," Physical Review Letters, vol. 79, pp. 3282–3285, 1997.

[3] M. Buchanan, M. Atakhorrami, J. F. Palierne, F. C. MacKintosh, and C. F. Schmidt, "High-frequency microrheology of wormlike micelles," Physical Review E, vol. 72, p. 011504, 2005.

[4] T. M. Squires and T. G. Mason, "Fluid mechanics of microrheology," Annual Review of Fluid Mechanics, vol. 42, pp. 413–438, 2010.

[5] N. Willenbacher and C. Oelschlaeger, "Dynamics and structure of complex fluids from high frequency mechanical and optical rheometry," Current Opinion in Colloid & Interface Science, vol. 12, pp. 43–49, 2007.

[6] M. Tassieri, M. Laurati, D. J. Curtis, D. W. Auhl, S. Coppola, A. Scalfati, K. Hawkins, P. R. Williams, and J. M. Cooper, "i-rheo: Measuring the materials' linear viscoelastic properties "in a step"!," Journal of Rheology, vol. 60, pp. 649–660, 2016.

[7] T. G. Mason, H. Gang, and D. A. Weitz, "Diffusing-wave-spectroscopy measurements of viscoelasticity of complex fluids," Journal of the Optical Society of America A, vol. 14, pp. 139–149, 1997.

[8] B. R. Dasgupta, S.-Y. Tee, J. C. Crocker, B. J. Frisken, and D. A. Weitz, "Microrheology of polyethylene oxide using diffusing wave spectroscopy and single scattering," Physical Review E, vol. 65, p. 051505, 2002.

[9] J. H. van Zanten, S. Amin, and A. A. Abdala, "Brownian motion of colloidal spheres in aqueous peo solutions," Macromolecules, vol. 37, pp. 3874–3880, 2004.

[10] A. A. Abdala, S. Amin, J. H. van Zanten, and S. A. Khan, "Tracer microrheology study of a hydrophobically modified comblike associative polymer," Langmuir, vol. 31, pp. 3944–3951, 2015.

[11] B. A. Krajina, C. Tropini, A. Zhu, P. DiGiacomo, J. L. Sonnenburg, S. C. Heilshorn, and A. J. Spakowitz, "Dynamic light scattering microrheology reveals multiscale viscoelasticity of polymer gels and precious biological materials," ACS Cent. Sci., vol. 3, pp. 1294–1303, 2017.

[12] M. Koziol, K. Fischer, and S. Seiffert, "Origin of the low-frequency plateau and the lightscattering slow mode in semidilute poly(ethylene glycol) solutions," Soft Matter, vol. 15, pp. 2666–2676, 2019.

[13] P. C. Cai, B. A. Krajina, M. J. Kratochvil, L. Zou, A. Zhu, E. B. Burgener, P. L. Bollyky, C. E. Milla, M. J. Webber, A. J. Spakowitz, and S. C. Heilshorn, "Dynamic light scattering microrheology for soft and living materials," Soft Matter, vol. 17, pp. 1929–1939, 2021.

[14] A. Palmer, T. G. Mason, J. Xu, S. C. Kuo, and D. Wirtz, "Diffusing wave spectroscopy microrheology of actin filament networks," Biophysical Journal, vol. 76, pp. 1063–1071, 1999.

[15] F. Amblard, A. Maggs, B. Yurke, A. N. Pargellis, and S. Leibler1, "Subdiffusion and anomalous local viscoelasticity in actin networks," Physical Review Letters, vol. 77, pp. 4470–4473, 1996.

[16] F. Gittes, B. Schnurr, P. D. Olmsted, F. C. MacKintosh, and C. F. Schmidt, "Microscopic viscoelasticity: Shear moduli of soft materials determined from thermal fluctuations," Physical Review Letters, vol. 79, pp. 3286–3289, 1997.

[17] T. Gisler and D. A. Weitz, "Scaling of the microrheology of semidilute f-actin solutions," Physical Review Letters, vol. 82,, pp. 1606–1609, 1999.

[18] N. Willenbacher, C. Oelschlaeger, M. Schopferer, P. Fischer, F. Cardinaux, and F. Scheffold, "Broad bandwidth optical and mechanical rheometry of wormlike micelle solutions," Physical

Review Letters, vol. 99, p. 068302, 2007.

[19] C. Oelschlaeger, M. C. P. Coelho, and N. Willenbacher, "Chain flexibility and dynamics of polysaccharide hyaluronan in entangled solutions: A high frequency rheology and diffusing wave spectroscopy study," Biomacromolecules, vol. 14, pp. 3689–3696, 2013.

[20] A. Papagiannopoulos, C. M. Fernyhough, and T. A. Waigh, "The microrheology of polystyrene sulfonate combs in aqueous solution," The Journal of Chemical Physics, vol. 123, p. 214904, 2005.

[21] A. Papagiannopoulos, T. A.Waigh, T. Hardingham, and M. Heinrich, "Solution structure and dynamics of cartilage aggrecan," Biomacromolecules, vol. 7, pp. 2162–2172, 2006.

[22] J. D. Ferry, Viscoelastic Properties of Polymers. USA: Wiley, third ed., 1980.

[23] R. M. Johnson, J. L. Schrag, and J. D. Ferry, "Infinite-dilution viscoelastic properties of polystyrene in θ-solvents and good solvents," Polymer Japanese, vol. 1, pp. 742–749, 1970.

[24] D. W. Hair and E. J. Amis, "Intrinsic dynamic viscoelasticity of polystyrene in and good solvents," Macromolecules, vol. 22, pp. 4528–4536, 1989.

[25] A. S. Lodge and Y. jing Wu, "Constitutive equations for polymer solutions derived from the bead/spring model of rouse and zimm," Rheologica Acta, vol. 10, pp. 539–553, 1971.

[26] K. Devanand and J. C. Selser, "Asymptotic behavior and long-range interactions in aqueous solutions of poly(ethylene oxide)," Macromolecules, vol. 24, pp. 5943–5947, 1991.

[27] V. K. Daga and N. J. Wagner, "Linear viscoelastic master curves of neat and laponite-filled poly(ethylene oxide)-water solutions," Rheologica Acta, vol. 45, pp. 813–824, 2006.

[28] K. W. Ebagninin, A. Benchabane, and K. Bekkour, "Rheological characterization of poly(ethylene oxide) solutions of different molecular weights," Journal of Colloid and Interface Science, vol. 336, pp. 360–367, 2009.

[29] D. Rivero, L. M. Gouveia, A. J. Müller, and A. E. Sáez, "Shear-thickening behavior of high molecular weight poly(ethylene oxide) solutions," Rheologica Acta, vol. 51, pp. 13–20, 2012.

[30] M. Gratz and A. Tschöpe, "Size effects in the oscillatory rotation dynamics of ni nanorods in poly(ethylene oxide) solutions," Macromolecules, vol. 52, pp. 6600–6612, 2019.

[31] M. Baumgärtel and N. Willenbacher, "The relaxation of concentrated polymer solutions," Rheologica Acta, vol. 35, pp. 168–185, 1996.

[32] P. E. Rouse, "A theory of the linear viscoelastic properties of dilute solutions of coiling polymers," Journal of Chemical Physics, vol. 21, pp. 1272–1280, 1953.

[33] P. G. de Gennes, Scaling Concepts in Polymer Physics. New York: Cornell University Press, 1979.

[34] M. Rubinstein and R. H. Colby, Polymer Physics. USA: Oxford University Press, first ed., 2003.

[35] M. Doi and S. F. Edwards, The Theory of Polymer Dynamics. Oxford: Oxford University Press, first ed., 1986.

[36] B. H. Zimm, "Dynamics of polymer molecules in dilute solution: Viscoelasticity, flow birefringence and dielectric loss," Journal of Chemical Physics, vol. 24, pp. 269–278, 1956.

[37] Equation 10 is obtained by taking the one-sided Fourier transform of the relaxation modulus and by ignoring proportionality constant.

[38] T. Kato, K. Nakamura, M. Kawaguchi, and A. Takahashi, "Quasielastic light scattering measurements of polystyrene latices and conformation of poly(oxyethylene) adsorbed on the latices," Polymer Journal, vol. 13, pp. 1037–1043, 1981.

[39] S. Kawaguchi, G. Imait, J. Suzuki, A. Miyahara, T. Kitanoll, and K. Ito, "Aqueous solution properties of oligoand poly(ethylene oxide) by static light scattering and intrinsic viscosity," Polymer, vol. 38, pp. 2885–2891, 1997.

[40] D. A. Weitz and D. J. Pine, "Diffusing-wave spectroscopy," in Dynamic Light Scattering: The Method and Some Applications (W. Brown, ed.), ch. 16, pp. 652–720, New York: Oxford University Press, 1993.

[41] D. N. Pinder, A. J. Swanson, P. Hebraud, and Y. Hemar, "Micro-rheological investigation of dextran solutions using diffusing wave spectroscopy," Food Hydrocolloids, vol. 20, pp. 240–244, 2006.

[42] T. Indei, J. D. Schieber, A. Córdoba, and E. Pilyugina, "Treating inertia in passive microbead rheology," Physical Review E, vol. 85, p. 021504, 2012.

[43] T. Indei, J. D. Schieber, and A. Córdoba, "Competing effects of particle and medium inertia on particle diffusion in viscoelastic materials, and their ramifications for passive microrheology," Physical Review E, vol. 85, p. 041504, 2012.

[44] R. M. L. Evans, M. Tassieri, D. Auhl, and T. A. Waigh, "Direct conversion of rheological compliance measurements into storage and loss moduli," Physical Review E, vol. 80, p. 012501, 2009.

[45] M. Tassieri, R. M. L. Evans, R. L. Warren, N. J. Bailey, and J. M. Cooper, "Microrheology with optical tweezers: data analysis," New Journal of Physics, vol. 14, p. 115032, 2012.

[46] M. Karim, S. C. Kohale, T. Indei, J. D. Schieber, and R. Khare, "Determination of viscoelastic properties by analysis of probe-particle motion in molecular simulations," Physical Review E, vol. 86, p. 051501, 2012.

[47] M. Karim, T. Indei, J. D. Schieber, and R. Khare, "Determination of linear viscoelastic properties of an entangled polymer melt by probe rheology simulations," Physical Review E, vol. 93, p. 012501, 2016.

[48] L.-H. Cai, S. Panyukov, and M. Rubinstein, "Mobility of nonsticky nanoparticles in polymer liquids," Macromolecules, vol. 44, pp. 7853–7863, 2011.

[49] In Fig. 8 left, red dashed line indicates $\xi = b' C_{\mathrm{p}}^{-\nu/(3\nu-1)}$ with $\nu = 0.588$ where prefactor b' was estimated by fitting with data (red dots), and blue dashed line represents $a = b'\sqrt{N_{\mathrm{e}}(1)} C_{\mathrm{p}}^{-\nu/(3\nu-1)}$ with $N_{\mathrm{e}}(1) = 13$ and the same b'. The values of b shown in text was derived from this b' by changing the polymer concentration from C_{p} to ϕ.

[50] F. Oesterhelt, M. Rief, and H. E. Gaub, "Single molecule force spectroscopy by afm indicates helical structure of poly(ethylene-glycol) in water," New Journal of Physics, vol. 1, pp. 6.1–6.11, 1999.

[51] In Fig. 8 right, red dashed line indicates $\tau_\xi = \tau_0' C_{\mathrm{p}}^{-3\nu/(3\nu-1)}$ where prefactor τ_0' was estimated by fitting with data (red dots), and blue dashed line represents $\tau_{\mathrm{e}} = \tau_0' N_{\mathrm{e}}(1)^2 C_{\mathrm{p}}^{-3\nu/(3\nu-1)}$ with the same τ_0'. The values of τ_0 shown in text was derived from this τ_0' by changing the polymer concentration from C_{p} to ϕ.